Ultra-compact terahertz switch with graphene ring resonators*

Jian-Zhong Sun(孙建忠)[1,2], Le Zhang(章乐)[2,†], and Fei Gao(高飞)[1]

[1] College of Computer Science & Technology, Zhejiang University of Technology, Hangzhou 310023, China
[2] Centre for THz Research, China Jiliang University, Hangzhou 310018, China

(Received 25 March 2016; revised manuscript received 26 May 2016; published online 25 August 2016)

We propose and numerically demonstrate a compact terahertz wave switch which is composed of two graphene waveguides and three graphene ring resonators. Changing the bias voltage of the Fermi level in the center graphene ring, the resonant mode can be tuned when the plasmon waves in the waveguides and rings are coupled. We theoretically explain their mechanisms as being due to bias voltage change induced carrier density of graphene modification and the coupling coefficients of graphene plasmon effect after carrier density change, respectively. The mechanism of such a terahertz wave switch is further theoretically analyzed and numerically investigated with the aid of the finite element method. With an appropriate design, the proposed device offers the opportunity to 'tune' the terahertz wave ON–OFF with an ultra-fast, high extinction ratio and compact size. This structure has the potential applications in terahertz wave integrated circuits.

Keywords: graphene, terahertz wave switch, surface plasmon

PACS: 87.50.U–, 96.12.kc **DOI:** 10.1088/1674-1056/25/10/108701

1. Introduction

Terahertz science and technology is undergoing a period of rapid development and diversified applications in security detection, imaging, sensing, and communication.[1–3] These applications demand many kinds of high-performance terahertz wave functional components such as filters, splitters, modulators, switches, phase shifter, and absorbers.[4–7] Among the terahertz wave functional devices required, manipulation of terahertz wave power exhibits tremendous potential applications in terahertz technology. In recent years, several types of terahertz wave switches have been reported in the literature.[8–10] The long size terahertz switch imposes limitations on the achievable density of integration circuits.[8] Moreover, the slow time response of the mechanically, thermally, or electrically tunable method has greatly restricted the practical application of the terahertz wave switch. Therefore, there is still a great challenge to realize a compact switch in the terahertz region. To the best of our knowledge, the rapid development of terahertz wave integrated circuit technology requires a large number of compact terahertz wave switches. To reduce the device size, a terahertz switch based on graphene is very desirable, but still lacking to date.

In recent years, graphene has aroused a great deal of research interest because of its outstanding electronic transport properties and optical properties. Due to this, graphene has been envisioned to facilitate new possibilities for constructing low power, rapidly tunable devices from the infrared to terahertz range.[11–13] Currently, many researchers are focusing on the issue of localized and propagated properties of graphene surface plasmon polaritons (SPPs), such as nano-discs, nano-ribbons, and graphene metamaterials.[14–17] Interestingly, it has been reported that some kinds of dynamically tunable infrared optical devices are based on graphene metasurfaces,[18] graphene metamaterial,[19] graphene nanostrips,[20] and graphene nanocrosses[21] respectively. These provide the possibility of devising flexibly tunable plasmon devices based on graphene. In addition, a mid-infrared fast-tunable graphene ring resonator has also been numerically analyzed.[22] It can also be used to construct a tunable mid-infrared filter, modulator, directional coupler and so on. Especially, the relaxation time of carriers in graphene is a few picoseconds, which offers great opportunities for ultra-fast terahertz manipulation devices.[23] In this study, we investigate and demonstrate a novel terahertz switch based on three graphene ring resonators. By tuning the bias voltage on the center graphene ring, its chemical potential and mode effective index can be tuned significantly which plays a role in controlling the transmission characteristics of the SPP wave. The device is investigated in detail using the finite element method (FEM) with COMSOL, a commercial finite element based software package. The calculation results indicate that the transmission characteristics of the resonant mode can feasibly be tuned by varying the radius or Fermi level of the center graphene ring. The results show that the ON–OFF response time is less than 1.2 ms and the attenuation of the novel terahertz wave switch is more than 17 dB at a frequency of 7 THz. We believe that our studies will be of value in fabricating the versatile, fast-tunable integrated devices in the terahertz region for terahertz wave communication and processing.

*Project supported by the Public Technology Research Project of Zhejiang Province, China (Grant No. 2015C31116).
†Corresponding author. E-mail: zhangle85@foxmail.com
© 2016 Chinese Physical Society and IOP Publishing Ltd

2. Device structure and theory analysis

In this study, we consider the structure, which is composed of two graphene waveguides and three graphene rings of which one has an inner radius of $R_1 = 0.2$ μm and the other two have an inner radius of $R = 0.5$ μm each. The coupling distance between ring and graphene waveguide is denoted by $d_1 = 0.1$ μm. Similarly, the distance between rings is denoted by $d_2 = 0.05$ μm. The SPP wave of the monolayer graphene is injected from the input port of the lower graphene waveguide and outputs from the upper graphene waveguide. The length of the graphene waveguide is $L = 2.6$ μm. The whole graphene structure is arranged on a polymethyl methacrylate medium with a refractive index of 1.48. The equivalent permittivity of graphene is given by $\varepsilon_{\rm eq} = 1 + {\rm j}\,\sigma_{\rm g}/(\varepsilon_0 \Delta\omega)$,[24,25] where j is the imaginary unit, $\sigma_{\rm g}$ represents the graphene surface conductivity, ε_0 is the permittivity of free space, Δ is the thickness of the graphene thin film, and ω is the angular frequency. The surface conductivity $\sigma_{\rm g}$ is governed by the Kubo formula including the interband and intraband transition contributions.[26,27] Here, only the transverse magnetic (TM) polarized SPP supported by monolayer graphene is considered in the investigation. The dispersion relation of TM wave along the graphene layer can be given by $\beta^2 = k_0^2[1-(2/\eta_0\sigma_{\rm g})^2]$,[28] where $k_0 = 2\pi/\lambda$ and $\eta_0 = 120\pi\Omega$ are the free space wavenumber and the intrinsic impedance of free space, respectively. The effective mode index, a parameter closely related to the confinement of TM wave, is calculated from $n_{\rm eff} = \beta/k_0$. The propagation length is defined as $L_{\rm spp} = 1/{\rm Im}(\beta)$, featuring the SPP propagation loss in graphene. Interestingly, the $L_{\rm spp}$ varies greatly when the chemical potential $\mu_{\rm c}$ is slightly changed, which is the guidance for designing the active surface plasmon wave devices. Graphene is modelled as a thin layer of $\Delta = 0.34$ nm in thickness[29] and its optical parameters are determined via the relative permittivity. In the near-field coupling case, the propagation loss on the graphene waveguide between two resonators is ignored 'for separation d_2 and the ${\rm Im}(\beta)$ are small enough. We make a subtle, yet important, distinction between the cavity buildup and magnification factor. The buildup factor is the ratio of the internal field in a particular graphene resonator to that in another resonator. The electric-field buildup factors are given by[30]

$$\beta_1(\varphi_1) = \frac{E_1}{E_2} = \frac{E_1}{E_3} = \frac{{\rm j}t_1 a_1 {\rm e}^{{\rm j}\varphi_1}}{1 - r_1 a_1 {\rm e}^{{\rm j}\varphi_1}}, \tag{1}$$

$$\beta_2(\varphi_1,\varphi_2) = \frac{E_2}{E_{\rm in}} = \frac{{\rm j}t_2 a_2 \tau_1(\varphi_1){\rm e}^{{\rm j}\varphi_2}}{1 - r_2 a_2 \tau_1(\varphi_1){\rm e}^{{\rm j}\varphi_2}}, \tag{2}$$

$$\beta_3(\varphi_1,\varphi_3) = \frac{E_3}{E_{\rm out}} = \frac{{\rm j}t_3 a_3 \tau_1(\varphi_1){\rm e}^{{\rm j}\varphi_3}}{1 - r_3 a_3 \tau_1(\varphi_1){\rm e}^{{\rm j}\varphi_3}}, \tag{3}$$

where

$$\tau_1(\varphi_1) = \frac{E_2^+}{E_2^-} = \frac{r_1 - a_1 {\rm e}^{{\rm j}\varphi_1}}{1 - r_1 a_1 {\rm e}^{{\rm j}\varphi_1}}$$

is the complex transmittivity through the No. 1 graphene ring (i.e. the lower graphene ring). $\varphi_i = 2\pi n_i L_i/\lambda_0 = \omega_i \tau_i^{\rm (RT)}$, are the single-pass phase-shifts of the i-th graphene ring ($i = 1$, 2, 3 specifies Nos. 1–3 graphene ring), r_i and t_i are the coupling reflection and transmission coefficient of the i-th graphene ring, respectively, $a_i = \exp(-\alpha_i L_i/2)$ is the single-pass attenuation coefficient of the i-th graphene ring, n_i is the refractive index of the i-th graphene ring, α_i is the loss coefficients of the i-th graphene ring, L_i is the circumference of the i-th graphene ring resonator, the electric fields E_i^- (just before) and E_i^+ (just after) are the electric fields in the i-th graphene ring resonator, E_{1i}^- and E_{1i}^+ are the electric fields in the No. 1 graphene ring resonator close to the i-th graphene ring resonator shown in Fig. 1. Note that the angular resonance frequency ω_i is related to the single pass phase shift according to $\varphi_i = \omega_i \tau_i^{\rm (RT)}$, where $\tau_i^{\rm (RT)}$ is the round-trip times of the i-th graphene ring resonator. Hence φ_i is indicative of the detuning of the input frequency from the resonance frequency.

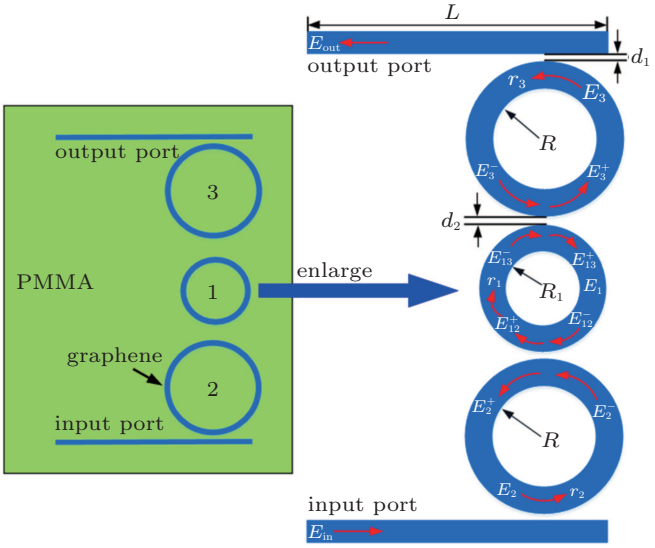


Fig. 1. (color online) Schematic diagram of the terahertz switch consisting of two graphene waveguides and three graphene rings.

The electric-field magnification factors are related to the buildup factors by the relations

$$\mu_2(\varphi_1,\varphi_2) = \frac{E_2}{E_{\rm in}} = \beta_2(\varphi_1,\varphi_2), \tag{4}$$

$$\mu_1(\varphi_1,\varphi_2) = \frac{E_1}{E_{\rm in}} = \frac{\beta_2(\varphi_1,\varphi_2)\beta_1(\varphi_1)}{\tau_1(\varphi_1)a_{22}}{\rm e}^{-{\rm j}\varphi_{22}}, \tag{5}$$

$$\mu_3(\varphi_1,\varphi_3) = \frac{E_3}{E_{\rm out}} = \beta_2(\varphi_1,\varphi_2), \tag{6}$$

$$\mu_4(\varphi_1,\varphi_3) = \frac{E_1}{E_{\rm out}} = \frac{\beta_3(\varphi_1,\varphi_3)\beta_1(\varphi_1)}{\tau_1(\varphi_1)a_{33}}{\rm e}^{-{\rm j}\varphi_{33}}, \tag{7}$$

where a_{22} and φ_{22} represent the attenuation and phase shift during the propagation from the No. 1 graphene ring coupling back to the No. 2 graphene ring (i.e. the center graphene ring), respectively; a_{33} and φ_{33} represent the attenuation and phase

shift during propagation from the No. 3 graphene ring coupling back to the No. 1 graphene ring, respectively. We set a bias voltage to the center graphene ring, by tuning the applied bias voltage, the graphene chemical potential can be changed significantly which plays a role in controlling the transmission characteristics of the SPP wave.

3. Simulation results and discussion

The two-dimensional numerical simulations are carried out in the present terahertz switch configurations by using the finite element method with the aid of the commercial software module COMSOL Multiphysics. Graphene SPPs are computed by the boundary mode analysis, propagating from one port to another, and perfectly matched layers allow scattering into eventual radiative modes in the transversal direction. Figure 2 shows the transmission spectra for the center graphene ring with various radius (R_1). One can see that the spectra in Fig. 2 'tend to be red-shifted' with the increase of R_1, which evidently validates the proportional relationship between the center frequency of the resonator and the radius of the center graphene ring. In order to explore the physical essence of the observed transmission spectra, we visually illustrate the electric-field (E_y) distributions of the SPPs at 7 THz corresponding to the different values of ring radius (R_1) of the center graphene ring as shown in Figs. 3(a)–3(c). One can obviously see that the SPP wave can be excited and confined strongly on a graphene ring at 7 THz when the resonance condition is satisfied. For the case of $R_1 = 0.20$ μm, most of the incident energy is trapped in the ring. At this time, the incident terahertz wave energy can successfully pass through the three graphene rings with sharp transmission bandwidth.

In order to investigate the coupling effect of the present configuration quantitatively, figure 4 shows the normalized transmissions of the terahertz switch with different chemical potential values in the center graphene ring. From Fig. 4, one sees that the SPP wave transmission ratio is over 87.1% at a

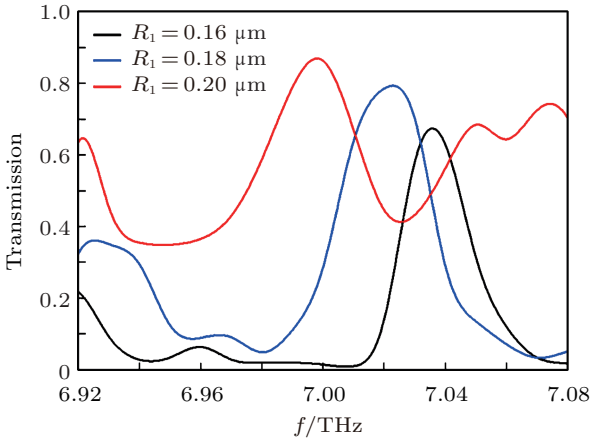


Fig. 2. (color online) Transmission spectra of the present terahertz switch for the three different values of center graphene ring radius (R_1).

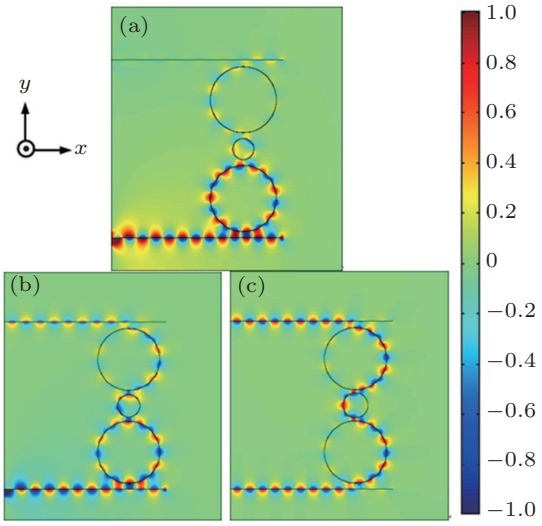


Fig. 3. (color online) Snapshots of E_y intensity distribution at 7 THz for central graphene ring radius (a) $R_1 = 0.16$ μm, (b) $R_1 = 0.18$ μm, (c) $R_1 = 0.20$ μm.

frequency of 7 THz when $\mu_c = 0$ eV. But, when $\mu_c = 0.2$ eV, the transmission is low to 0.2%. That is to say, by changing the chemical potential value of the center graphene ring, the coupling mode in the ring resonator can be significantly tuned. It can be noted that when the resonance condition is satisfied, most of the incident energy can efficiently be obtained through the output graphene waveguide. The simulation results of electric field distribution of the SPPs in the plasmonic structure with the different chemical potentials at $f = 7$ THz are presented in Fig. 5. The incident signal is injected through the left port of the lower graphene waveguide. The electric field distribution clearly shows the coupling process of SPPs among the graphene rings. Note that the electric field intensities are uniformly distributed in the two parallel graphene waveguides and three graphene rings without any back scattering. In Fig. 5(a), one can see that when the resonance condition is satisfied, the incident energy which is trapped in the ring resonator couples to the output port of the lower graphene waveguide almost simultaneously. Since the surface conductivity of graphene is tunable by changing the chemical potential, the energy flow in two parallel graphene waveguides and three graphene rings can be controlled by bias voltage. When the central graphene ring in the three graphene rings system is biased, its Fermi level, and hence the surface conductivity, should be modified accordingly. Supposing that a bias voltage yields a chemical potential of $\mu_c = 0.1$ eV in the center graphene ring, the SPPs from the input graphene waveguide will be partly coupled to the lower one which is finally collected by output port (see Fig. 5(b)). Similarly, if a bias voltage (i.e., a chemical potential of $\mu_{c2} = 0.2$ eV) is added onto the center graphene ring, the biased graphene ring will behave as a dielectric and cannot support the plasmonic mode, the incident energy from the lower graphene waveguide cannot

be coupled to the upper graphene waveguide output as demonstrated in Fig. 5(c). Since the resonance condition in three graphene rings is not satisfied, the terahertz wave cannot propagate efficiently through the three graphene rings to the upper graphene waveguide output. From Fig. 5, one can see that there would be different electric field intensities in the output port of the present device for different bias voltages. Accordingly, the structure forms an effective terahertz wave switch. Here, we define the extinction ratio of the proposed device as $\mathrm{ER} = -10\log(P_{\mathrm{out}}/P_{\mathrm{in}})$, where P_{in} and P_{out} represent the power flows of input and output port, respectively. In this paper, the extinction ratio is 17.7 dB. Furthermore, the controlling rate is related to not only the response time of graphene material, but also the system response time. In order to analyze the time domain steady state intensity response of the presented terahertz wave switch, a continuous wave is excited at the input port position. Figure 6 shows the corresponding time domain steady state intensity response, and the switching rate of the proposed device is as short as around 1.2 ms, which is about

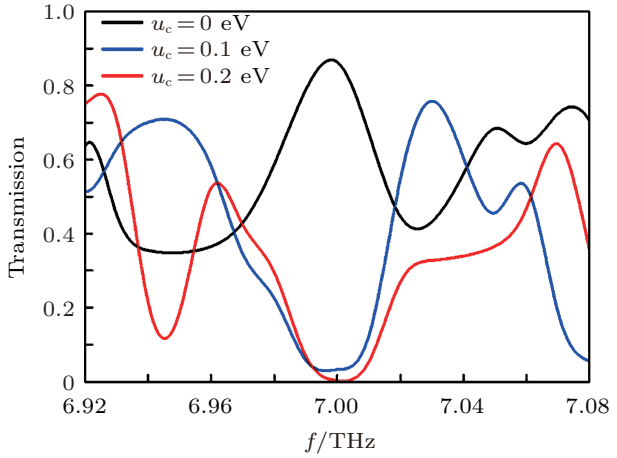


Fig. 4. (color online) Transmission characteristics of the terahertz switch with different chemical potential values of the center graphene ring.

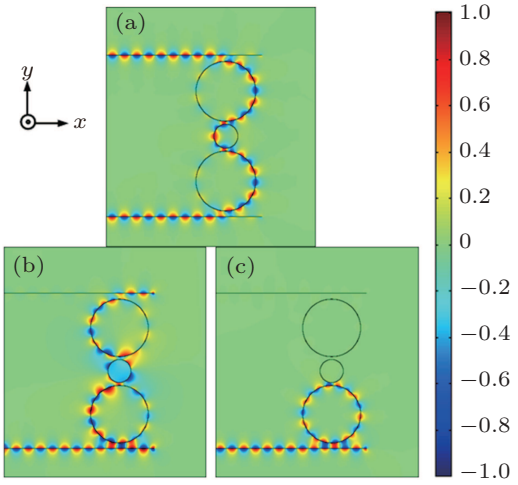


Fig. 5. (color online) Snapshots of E_y intensity distribution at 7 THz for different chemical potential values of the center graphene ring: (a) $\mu_c = 0$ eV, (b) $\mu_c = 0.1$ eV, (c) $\mu_c = 0.2$ eV.

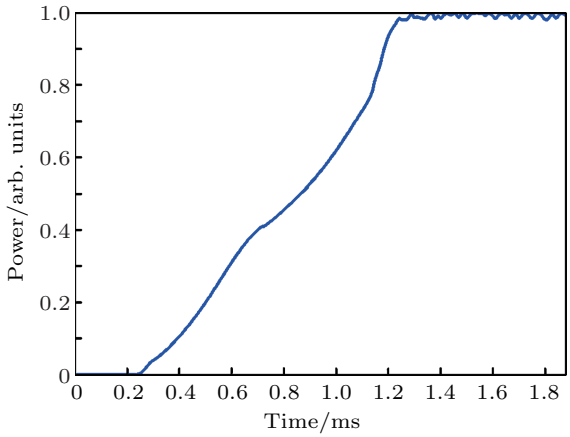


Fig. 6. (color online) Time domain steady state terahertz wave intensity response.

1/10 response time of a previous terahertz switch.[8] These results can be valuable references for studying the ultrafast response terahertz wave switches.

4. Conclusions

We numerically investigate the design and transmission characterization of terahertz wave switch based on graphene rings and waveguides. Since the surface conductivity of graphene is tunable by gate voltage, the coupling process can be controlled. When the center graphene ring is biased, its chemical potential hence the surface conductivity should be accordingly modified. By varying the Fermi level or radius of the center ring resonator, SPP wave strongly confined in the graphene ring can be tuned feasibly. The simulated results show that the terahertz wave transmission ratio can be tuned from 87.1% to 1.7% with the chemical potential in the center graphene ring changing from 0 eV into 0.2 eV. These results are consistent with our theoretical predictions. We believe that the proposed terahertz wave switch can be useful for future terahertz wave communication systems.

Acknowledgment

The authors thank Prof. J Li for his useful discussion.

References

[1] Jepsen P, Cooke D and Koch M 2011 *Laser Photon. Rev.* **5** 124
[2] Federici J and Moeller L 2010 *J. Appl. Phys.* **107** 111101
[3] Tonouchi M 2007 *Nat. Photon.* **1** 97
[4] Hung H, Wu C and Chang S 2011 *J. Appl. Phys.* **110** 093110
[5] Lin W, Wu C, Yang T and Chang S 2010 *Opt. Express* **18** 27155
[6] Woo J, Kim M, Kim H and Jang J 2014 *Appl. Phys. Lett.* **104** 081106
[7] Lin X, Wu J, Hu W, Zheng Z, Wu Z, Zhu G, Xu F, Jin B and Lu Y 2011 *AIP Adv.* **1** 032133
[8] Li J and Yao J 2008 *Opt. Commun.* **281** 5697
[9] Zhang H, Guo P, Chen P, Chang S and Yuan J 2009 *J. Opt. Soc. Am. B* **26** 101
[10] Yuan Y, He J, Liu J and Yao J 2010 *Appl. Opt.* **49** 6092
[11] Gan C, Chu H and Li E 2012 *Phys. Rev. B* **85** 125431
[12] Vakil A and Engheta N 2011 *Science* **332** 1291
[13] Ding G W, Liu S B, Zhang H F, Kong X K, Li H M, Li B X, Liu S Y and Li H 2015 *Chin. Phys. B* **24** 118103

[14] Lee S H, Choi M, Kim T, Lee S, Liu M, Yin X, Choi H, Lee S S, Choi C, Choi S, Zhang X and Min B 2012 *Nat. Mater.* **11** 936
[15] Liu M, Yin X, Ulin-Avila E, Geng B, Zentgraf T, Ju L, Wang F and Zhang X 2011 *Nature* **474** 64
[16] Alaee R, Farhat M, Rockstuhl C and Lederer F 2012 *Opt. Express* **20** 28017
[17] Zhu X, Yan W, Mortensen N and Xiao S 2013 *Opt. Express* **21** 3486
[18] Cheng H, Chen S, Yu P, Liu W, Li Z, Li J, Xie B and Tian J 2015 *Adv. Opt. Mater.* **3** 1744
[19] Cheng H, Chen S, Yu P, Li J, Xie B, Li Z and Tian J 2013 *Appl. Phys. Lett.* **103** 223102
[20] Cheng H, Chen S, Yu P, Duan X, Xie B and Tian J 2013 *Appl. Phys. Lett.* **103** 203112
[21] Cheng H, Chen S, Yu P, Li J, Deng L and Tian J 2013 *Opt. Lett.* **38** 1567
[22] Huang Z, Wang L, Sun B, He M, Liu J, Li H and Zhai X 2014 *J. Opt.* **16** 105004
[23] Dawlaty J, Shivaraman S, Chandrashekhar M, Rana F and Spencer M 2008 *Appl. Phys. Lett.* **92** 042116
[24] Brar V, Jang M, Sherrott M, Lopez J and Atwater H 2013 *Nano Lett.* **13** 2541
[25] Yan H, Low T, Zhu W, Wu Y, Freitag M, Li X, Guinea F, Avouris P and Xia F 2013 *Nat. Photon.* **7** 394
[26] Koppens F, Chang D and García A 2011 *Nano Lett.* **11** 3370
[27] Zhang Y, Liu T, Meng B, Li X, Liang G, Hu X and Wang Q 2013 *Nat. Commun.* **4** 1811
[28] Liu P, Cai W, Wang L, Zhang X and Xu J 2012 *Appl. Phys. Lett.* **100** 153111
[29] Xia S, Zhai X, Wang L, Lin Q and Wen S 2016 *Opt. Express* **24** 427
[30] Smith D, Lepeshkin N, Schweinsberg A, Gehring G, Boyd R, Park Q, Chang H and Jackson D 2006 *Opt. Commun.* **264** 163